Desalination and Water Treatment
www.deswater.com
doi: 10.5004/dwt.2019.24223

158 (2019) 319–329
August

Synthesis of porous iron – zirconium mixed oxide fabricated ethylene diamine composite for removal of cationic dye

Roshni Kumari, Soumen Dey*

Centre for Applied Chemistry, Central University of Jharkhand, Ranchi-835205, Jharkhand, India, Tel. +91 9661399711; emails: soumen.dey@cuj.ac.in, soumdey@gmail.com (S. Dey), roshnikumari311@gmail.com (R. Kumari)

Received 23 September 2018; Accepted 4 April 2019

ABSTRACT

Synthesis of iron-zirconium binary oxide fabricated ethylene diamine (IZBO-en) composite involved two step synthesis including mixed binary oxide synthesis followed by synthesis of binary oxide-ethylene diamine composite. Mixed binary oxide was synthesized by co-precipitation method using ammonia as neutralizing agent. Binary oxide based ethylene diamine composite was synthesized using sodium dodecyl sulfate and potassium persulfate as reagents in reaction. Yield of product was 88%. Characterization of the material was done using Fourier-transform infrared spectroscopy, scanning electron microscopy, and Brunauer–Emmett–Teller analysis. Surface area was found to be 54.74 $m^2 g^{-1}$. The synthesized material was efficient for removal of cationic dye methylene blue which is known for its toxicological effects. Adsorption parameters like contact time, dose, interference and pH were studied. Maximum adsorption capacity was found to be 242.79 mg g^{-1}. Kinetic data suggested the mechanism of adsorption follows pseudo-second-order rate (R^2 = 0.998) with a rate constant of 2.788 mg g^{-1} min^{-1} and follows Langmuir adsorption isotherm model (R^2 = 0.987). Thermodynamic study revealed the process to be spontaneous and feasible with large negative free energy (ΔG = –9.54 kJ mol^{-1}). Column study shows a removal of 600 ml 2 mg L^{-1} with 1 g material. Desorption was achieved with 79% regeneration in acidic medium. Real wastewater from nearby textile industry was tested and found to get decolourized with the material. In conclusion, IZBO-en can be efficiently used in detoxification of cationic dyes.

Keywords: Binary oxide; Ethylene diamine; SEM; Adsorption; Kinetics

1. Introduction

The rapid growth of population coupled with increased industrialization leads to scarcity of pure water [1]. Water contamination with organic compounds and heavy metals is becoming a serious health concern. Dyes are used in wide variety of important industries, including but not limited to: textiles, paper, pigment, paint, plastic, leather, food and beverages, cosmetic and pharmaceuticals [2]. Dyes are large complex aromatic compounds which are non-biodegradable and have carcinogenic effect [3]. Besides its detrimental effect to mankind, dyes impose serious threat to biological processes inside water bodies as the colour of dyes prevents penetration of sunlight [4]. Hence there is a need for removal of toxicity from wastewater. Large number of treatment methods used widely for removal of toxicity [5–10]. Adsorption has proved to be of uttermost importance in recent years for wastewater treatment because of easy implementation, cost-effectiveness and simple procedures [11–15]. A wide variety of adsorbents like metal oxides [16], activated carbon [17,18], biomass [19,20], polymer, nanosilicates, nanoferrites, resins etc. were extensively used [21–27]. Polymer-based adsorbents are used worldwide for remediation of wastewater due to their high stability,

* Corresponding author.

porosity and large adsorption capacities [6]. Preferably, polymers and composites containing reactive amine groups could easily interact with the medium and hence find wide applications in removal of toxic dyes from wastewater [6–29]. Recently many green synthesized nanoparticles were used for the removal of toxic organic and inorganic pollutants [30].

The use of magnetic metal oxide based adsorbents attracted the researchers in recent years due to their higher surface area and low diffusion resistance. Hence, several modifications on iron oxide nanoparticles are still interesting and will continue to be a part of modern research [31,32]. The fusion of ethylenediamine with the magnetic nanoparticles enhances its chelating tendency, improves stability and complexation with the adsorbent molecules. Considering above aspect, an iron-zirconium binary oxide fabricated ethylene diamine (IZBO-en) composite was prepared by two step syntheses [33,34].

2. Experimental section

Mixed binary oxide nanoparticles of iron and zirconium were synthesized by general precipitation method using iron and zirconium salts. The mixed oxide was then fabricated with ethylene diamine using potassium persulfate (KPS) and sodium dodecyl sulfate (SDS) as reagents in reaction [35]. The present work corresponds to the batch and column study of Methylene blue (MB) by the synthesized composite. The batch test was done to determine the adsorption efficiency at different parameters like dose, concentration pH and interference by co-existent ions. Column study was done for the estimation of throughput volume and evaluation on industrial scale.

2.1. Chemicals and methods

Ferric nitrate [$Fe(NO_3)_3$], Zirconyl oxychloride [$ZrOCl_2.8H_2O$], Hydrochloric acid, ammonia solution, Ethylene Diamine, acetone, KPS and SDS was received from Rankem chemicals (India). MB dye (spectrochem) was used as received for stock solution preparation.

2.1.1. Synthesis of Fe_2O_3–$ZrO_2.xH_2O$ binary oxide (IZBO)

5g of ferric nitrate and 5g of Zirconium oxychloride octahydrate was separately dissolved in 30 ml of 0.1 M hydrochloric acid and mixed together. 30% ammonia solution was dropwise added till complete precipitation. After complete precipitation, the precipitate was left for aging for 2 d for setting of particles. Finally the precipitate was filtered through sintered bed, washed several times and dried at 80°C in oven for 10 hr.

2.1.2. Synthesis of IZBO-en composite material

2.2 ml of ethylene diamine was added in round bottom flask containing 30 ml of HCl, 1.5 g of synthesized binary oxide was added to this solution. 3 g of SDS dissolved in 30 ml chloroform was added into the flask. The reaction mixture was sonicated for 1 h in ultrasonic bath. 1.5 g of KPS was dissolved in 20 ml water and added drop wisely to the stirring reaction mixture for 30 min and stirring was continued for 24 h. Acetone was added to quench the reaction. The binary oxide based ethylene diamine composite thus obtained was washed with methanol and water to remove unreacted materials. Finally it was dried at 60°C for 8 h in vacuum oven and kept in desiccator for characterization and further application. The product was obtained in 88% yield.

2.2. Instrumentation

Analytical balance (Denver Instrument Corporation, USA) was used for weighing of samples. Systronic digital pH meter 802 (India) was used for pH measurements. Sohag orbital shaker incubator was used for shaking and muffle furnace (Thermo-Scientific, Philippines) for drying of samples. ZIESS (Germany) scanning electron microscopy (SEM) Analyzer for SEM study and Hitachi double beam U-2900 (Japan), equipped with ultraviolet (UV) solutions program NSJ for all UV measurements. Perkin Elmer spectrum-II (USA) and Remi-bench top centrifuge, India (R-8 M) were used for Fourier-transform infrared spectroscopy (FTIR) analysis and centrifugation respectively. Micromeritics 3 Flex surface analyzer, USA (Version 3.02) was used for Brunauer–Emmett–Teller (BET) analysis.

2.3. Batch adsorption procedure

Molecular formula of MB is $C_{16}H_{18}ClN_3S$; molar mass is 319.85 and λ_{max} at 664 nm. Each experimental setup used 0.2 g of the synthetic adsorbent added to 50 ml of MB solution of known concentration. The batch mode was conducted with MB solution without pH adjustment (pH 6.5) [36]. 5 mg L^{-1} MB shows pH 6.5 and it was used as such for further experiment. 0.2 g of adsorbent was used and mechanical shaking was performed for 120 min. The shaking was followed by centrifugation at 3,000 rpm for 3 min to separate the adsorbent from the adsorbent. The absorbance recorded by UV-vis spectrophotometer gave the percentage adsorption and the adsorption capacity was calculated by the equation below

$$q_e = \left(C_i - C_e\right) \times \frac{V}{m} \tag{1}$$

where q_e = adsorption capacity, C_i and C_e were the initial and final concentration respectively, V is the volume of solution taken and m is the mass of adsorbent used. The similar setup was used for other parameters like concentration variation, dose, interference and pH keeping other conditions constant. All experiments were performed in triplicate set. For kinetic studies, a measured amount of composite (0.2 g) was added to 50 ml MB solution of known concentration (5 mg L^{-1}) at 298 K. Colourimetric measurements were done at various time intervals until the equilibrium was reached. For isotherm studies the reaction temperature and dye concentration was varied (293–303 K, 10–60 mg L^{-1}) keeping other parameters same. The study of thermodynamic was done at different temperature and dye concentration.

For desorption experiment a concentrated solution of MB (50 mg L^{-1}) was prepared and a measured amount of adsorbent (0.2 g) was added in 50 ml solution. It was kept for complete saturation of the material with dye in mechanical

shaker. The dye saturated material was separated and washed followed by drying. The concentrations before and after adsorption were measured. The dried dye loaded material was used for desorption test using two different media, that is, acidic (0.1 M HCl) and basic (0.1 M NaOH). The addition of the saturated material in these media was followed by overnight stirring. The desorbed material was separated and the amount of dye desorbed was calculated. Regenerated material was tested for re-use. Real wastewater sample was collected from textile industry and analysis was done to estimate the efficiency on industrial scale.

3. Result and discussion

The product was obtained with 88% yield as dark brown solid. Since 5 mg L^{-1} dye solution shows pH 6.5, this pH was set as working pH.

3.1. Effect of time

The effect of contact time on adsorption rate of dye with fixed adsorbent dose (0.2 g) was tested with a time interval of 20 min keeping other parameters constant. A rapid uptake (up to 86%) was noticed within first 20 min and attains maximum at 100 min (Fig. 1a).

3.2. Effect of dose

The effect of dose of synthetic adsorbent on adsorption of dye was observed for different adsorbent dose (0.1–0.6 g). There was a fast and effective adsorption upon moving from 0.1–0.4 g of adsorbent dose, thereafter an insignificant improvement was seen. The fast increase in adsorption percent from 76.8%–92.5% for 0.1–0.4 g dose might be attributed to the availability of greater number of active sites provided through increased dose of adsorbent while the slow increase from 92.5%–96.8% for 0.4–0.6 g dose might be due to the saturation of the active sites or it might be due to the hindrance provided by the loaded dye molecules to the approaching dye molecules (Fig. 1b) [37].

3.3. Effect of concentration

Different concentration of the dye was tested for removal efficiency by the adsorbent. A continuous decrease in adsorption was seen for the increased concentration of

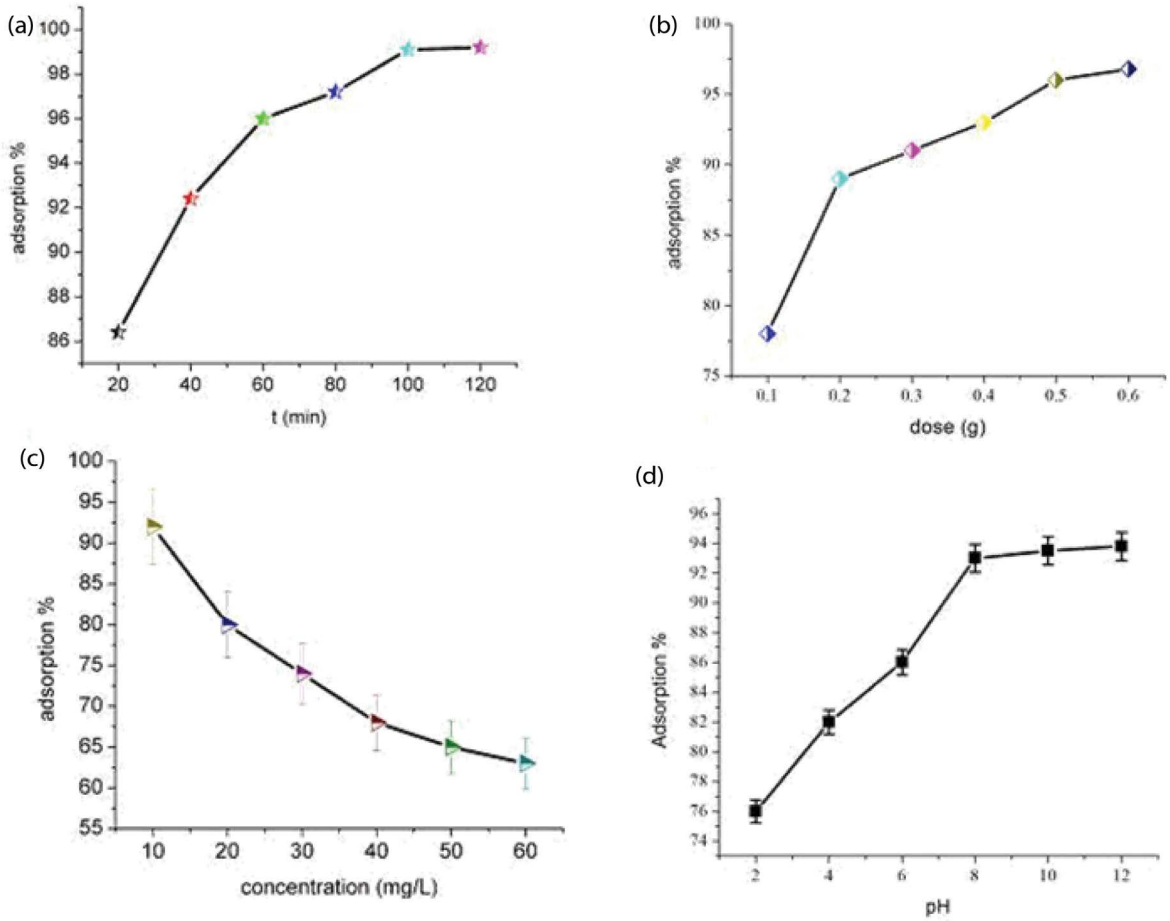

Fig. 1. (a) Effect of contact time on adsorption of MB on synthetic adsorbent (C_0 = 5 mg L^{-1}, pH = 6.5, T = 298 K), (b) Effect of dose on adsorption of MB on synthetic adsorbent (C_0 = 5 mg L^{-1}, pH = 6.5, T = 298 K), (c) Effect of concentration variation on adsorption of MB on synthetic adsorbent (C_0 = 10–60 mg L^{-1}, pH = 6.5, T = 298 K), and (d) Effect of pH on adsorption of MB on synthetic adsorbent (C_0 = 5 mg L^{-1}, pH = 2–12, T = 298 K).

the dye. Effect of initial concentration of MB on adsorption percent was studied by shaking varying concentration (10–60 mg L^{-1}) of 50 ml solution containing 0.2 g of adsorbent at pH 6.5 for 60 min. The adsorption percent decreases from 94.8% to 64.2% when the initial concentration of dye increased from 10–60 mg L^{-1} which might be explained on the basis that fewer number of active sites were available for greater number of MB molecules that resulted in faster saturation and reduced adsorption (Fig. 1c). However, the adsorption percent decreases while the uptake capacity increases with increasing concentration of the dye which might be due to the increase in the number of dye molecules adsorbed into the same dose of adsorbent [27].

3.4. Effect of interference

Since untreated industrial effluents contain some common salts along with the dye, this necessitates the study of effect of interference of co-existing ions on the adsorption efficiency of the material. The effect of interference was checked with different concentration of NaCl and Na_2SO_4. There was no such significant effect of interfering ions on adsorption percent.

3.5. Effect of pH

The process such as adsorption was well known to be a surface phenomenon and hence pH plays an important role in driving the process. The particular pH at which the batch adsorption experiment (except effect of pH test) performed was 6.5 (pH without adjustment). For the effect of pH, the experiments were carried out in pH range of 2–12.

The final pH of the solution was measured and compared with the initial pH and the results obtained showed near neutral pH range of the solution after adsorption. The variation of adsorption percent with pH is presented in Fig. 1d. Increase in adsorption efficiency with increase in pH was seen. It can be explained as follows: basic medium favours the increased adsorption of the cationic dye molecules onto the adsorbent surface. The increasing pH raised the concentration of negative charge on the adsorbent surface that resulted in increased adsorption of cationic dye. This can also be explained on the basis of pH_{pzc} value. The pH_{pzc} value for the composite was 6.1 that confirmed the negative charge on the surface of the composite material. Hence, at pH lower than 6.1, the positively charged surface limits the adsorption of cationic dye (poor electrostatic attractions) in acidic medium while at higher pH above 6.1, the cationic dyes were more attracted towards the negatively charged surface due to favored electrostatic attraction of the positively charged dye molecules towards the negatively charged surface [32,38,39].

3.6. Kinetic study

Kinetic model suggests the rate of reaction in terms of rate constant and adsorption capacity. Three common models namely pseudo-first-order (Eq. (2)), pseudo-second-order (Eq. (3)) and intra-particle diffusion (Eq. (4)) were tested.

$$\ln\left(q_e - q_t\right) = \ln q_e - k_1 t \tag{2}$$

$$\frac{t}{q_t} = \frac{1}{k_2} \times \frac{1}{q_e^2} + \frac{1}{q_e} \times t \tag{3}$$

$$q_t = k_i t^{0.5} + c \tag{4}$$

where q_e is the uptake capacity at equilibrium (mg g^{-1}), q_t is the amount of solute adsorbed at time t (mg g^{-1}), k is the rate constant. Calculated model constants were given in Table 1. The kinetics was best described by pseudo-second-order model with maximum R^2 (Table 1). Three kinetic plots were shown in Figs. 2a–c [11].

Mechanism was described by pseudo-first, pseudo-second and intra-particle diffusion model with the latter as the best fit model suggesting the adsorption to be interdependent on the adsorbent-adsorbate system and involved chemisorption with the chemical reaction between the adsorbate and the adsorbent as the rate determining step of the process. Intra-particle diffusion involves mass transfer of molecules from the surface to the pores of adsorbent and diffusion of dye into the active sites of the adsorbent. The intra-particle diffusion plot shows the straight line deviated from the origin confirm that this is not only the rate limiting step in the adsorption process [40–42].

3.7. Isotherm study

Isotherm models study reveals the interaction of dye with the adsorbent surface as a function of concentration at a particular temperature (at equilibrium: dose = 0.2 g, T = 298K, pH = 6.5, V = 50 ml). The analysis was done by linear and non-linear method to minimize the error occupancy and achieve accuracy. The maximum value of R^2 was obtained for Langmuir model which suggests homogenous interaction between the dye molecules and the adsorbent surface and also the model describes monolayer adsorption with identical sites and equivalent energy [43]. Linear plots for Langmuir, Freundlich and Dubinin-Radushkevich models were used for calculation of maximum adsorption capacity q_{max} and rate constant describing adsorption intensity (Figs. 3a–c). The results obtained for the best fit model (Langmuir) were found equivalent for both linear and non-linear methods [44]. The maximum adsorption capacity of 242.79 mg g^{-1} justifies the applicability of the porous adsorbent. Comparison of adsorption capacities with some literature is given (Table 2). The decrease in adsorption capacity with increasing temperature suggests the exothermic nature of the physico-chemical process.

The essential feature related with Langmuir model is R_L, which is the separation factor pertaining to the extent of ease with which adsorption could occur.

Table 1
Selected kinetic model constants

Order	q_e (mg g^{-1})	K	R^2
Pseudo-first	0.356	0.071 min^{-1}	0.961
Pseudo-second	1.284	2.788 mg g^{-1} min^{-1}	0.998
Intra-particle diffusion	0.984	0.035 mg g^{-1} $min^{-0.5}$	0.941

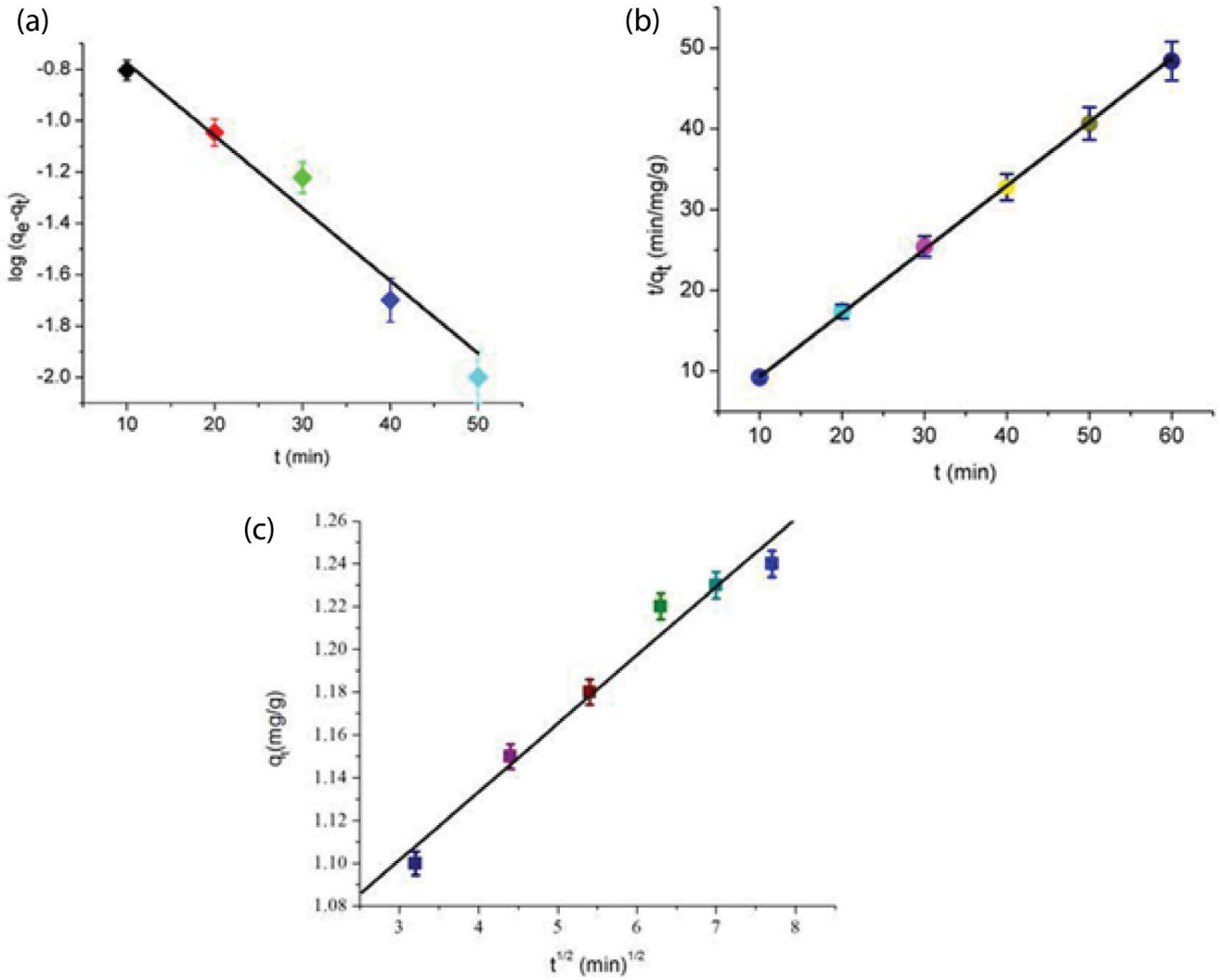

Fig. 2. (a) Pseudo-first-order plot, (b) pseudo-second-order plot, and (c) intra-particle diffusion plot.

$$R_L = \frac{1}{\left(1 + bC_m\right)} \tag{5}$$

where C_m is the maximum initial concentration of the dye and b is the Langmuir rate constant. The calculated value of R_L was 0.0062 which is in between 0 and 1 suggesting favourable adsorption [11].

The calculated values of various model constants using linear and non-linear methods were given in Table 3 and Table 4 respectively.

3.8. Thermodynamic study

Thermodynamic study suggests the nature of the occurrence of the adsorption process in terms of feasibility and type of heat change involved. The experimental data for different thermodynamic parameters are listed in Table 5.

The values of enthalpy ΔH and entropy ΔS were calculated through the slope and intercept of the plot corresponding to ln K vs. $1/T$. The free energy value was calculated using the general equation

$$\Delta G = \Delta H - T\Delta S \tag{6}$$

The negative values of ΔG (Table 5) suggest that the adsorption process to be thermodynamically feasible and spontaneous. The negative values of ΔH indicate exothermic nature of the process.

The degree of disorder or randomness is measured by entropy. The positive values of ΔS obtained for the present study signifies the rapid movement or disorder of the adsorbate particles at the interaction surface during the adsorption process [51].

3.9. Characterization

3.9.1. Fourier-transform infrared spectroscopy

FTIR analysis was used for detection of functional groups present in the adsorbent. The shift in the peaks before

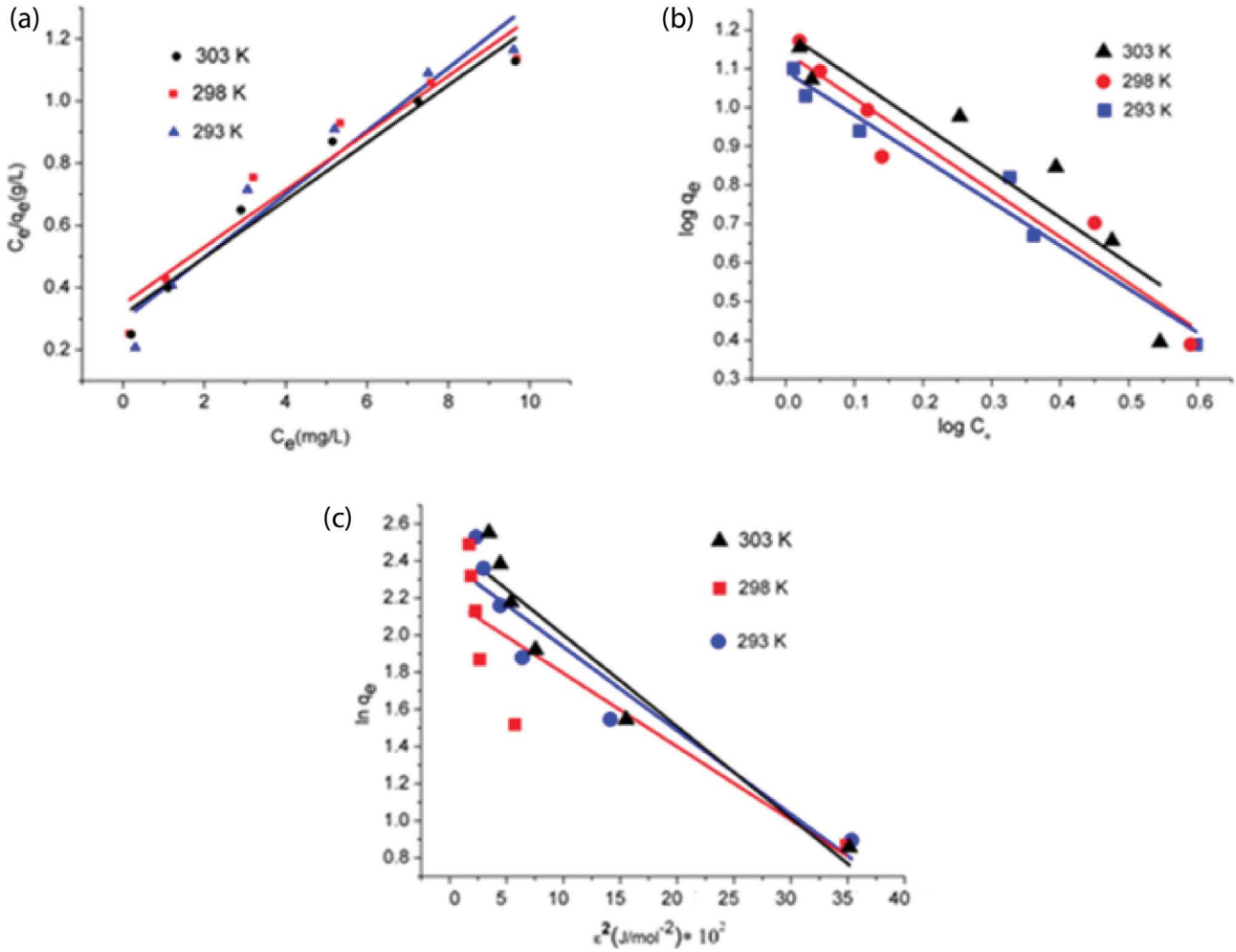

Fig. 3. (a) Langmuir isotherm plot, (b) Freundlich isotherm plot, and (c) D-R isotherm plot.

Table 2
Comparative adsorption capacities of various adsorbents

Adsorbent	Dye	Uptake (mg g^{-1})	Reference
MIL-53(Al)-NH_2	MB	208.3	Li et al., [45]
Fe_3O_4@MIL-100(Fe)	MB	73.80	Shao et al., [46]
NH_2-MIL-101(Al)	MB	188	Haque et al., [47]
Fe_3O_4@APS@AA-Co-CAMNPs	MB	142.9	Ge et al., [48]
Magnetite@Silica@pectin	MB	85.18	Attallah et al., [49]
Hybrid nanocomposite	MB	182	El-Shafey et al., [50]
Propylene diamine basic activated carbon			
IZBO-en	MB	242.79	Present work

and after adsorption describes the binding of dye molecules with the functional groups at the adsorbent surface. The spectra before and after adsorption were shown in Figs. 4a and b. The broad metal oxygen bonds are present in the range 400–600 cm^{-1}. The vibrations corresponding to tetrahedral and octahedral cations M–O bond were present in the range 550–600 cm^{-1} and 390–400 cm^{-1} respectively [52–54]. The shift in the peaks corresponding to the surface interaction of the adsorbent and the dye molecules were given in the Table 6.

3.9.2. Mechanism

The proposed mechanism for the described adsorption process is shown in Fig. 5. The mechanism suggests that

the adsorptive binding between the dye and the composite was based on the H – bonding between the N-atom of dye and the H-atom of the composite which was also supported by the data obtained for FTIR peaks. Moreover, the role of electrostatic attraction was seen in the adsorption process described which was supported by the kinetic data that suggested the process involved chemisorption (pseudo-second-order kinetic).

Table 3
Calculated values of isotherm model constants using linear method

Isotherm model	Temperature (K)		
Langmuir	293	298	303
q_0 (mg g^{-1})	242.79	213.87	214.49
b (L mg^{-1})	2.66	2.98	4.18
R^2	0.986	0.987	0.982
Freundlich			
K_F (mg g^{-1})	98.31	92.87	96.35
n	1.02	0.94	1.71
R^2	0.912	0.923	0.903
Dubinin-Radushkevich			
χ_m (mmol g^{-1})	2.82	2.54	3.42
β (mol^2 J^{-2})	4.51×10^{-3}	1.39×10^{-3}	6.63×10^{-3}
E (KJ mol^{-1})	0.92	0.17	0.13
R^2	0.881	0.791	0.892

Table 4
Calculated values of isotherm model constants using non-linear method

Isotherm model	Temperature (K)		
Langmuir	293	298	303
q_0 (mg g^{-1})	241.68	213.91	216.42
b (L mg^{-1})	2.61	1.77	3.68
R^2	0.989	0.988	0.992
Freundlich			
K_F (mg g^{-1})	98.31	92.87	96.35
n	1.98	0.64	1.22
R^2	0.922	0.929	0.933
Dubinin-Radushkevich			
χ_m (mmol g^{-1})	2.84	2.38	2.97
β (mol^2 J^{-2})	4.32×10^{-3}	1.89×10^{-3}	6.12×10^{-3}
E (KJ mol^{-1})	0.94	0.22	0.19
R^2	0.886	0.891	0.899

3.9.3. Scanning electron Microscopy – Energy-dispersive X-ray spectroscopy

The prominent peaks of the constituent elements in the material were obtained that justified the combination of the

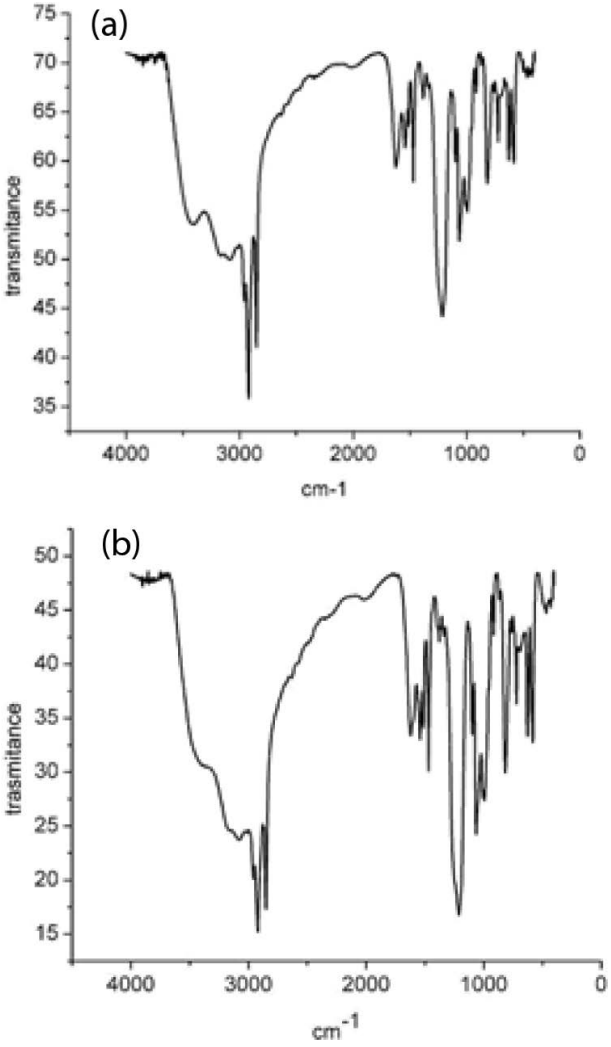

Fig. 4. (a) FTIR peaks before adsorption and (b) after adsorption.

Table 5
Experimental results of various thermodynamic parameters

Concentration (mg L^{-1})	Temperature (K)	ΔG (KJ mol^{-1})	ΔH (KJ mol^{-1})	ΔS (KJ mol^{-1} K^{-1})
10	293	–9.18	–1.83	0.32
	298	–9.35	–1.83	0.32
	303	–9.54	–1.83	0.32
20	293	–17.94	–2.22	0.62
	298	–18.25	–2.22	0.62
	303	–18.56	–2.22	0.62

Table 6
Group frequencies of various functionalities before and after adsorption

Before adsorption (cm^{-1})	After adsorption (cm^{-1})	Group frequencies
3,420	3,400	Alcohol, H-bonded O–H Stretching (broad)
2,865	2,848	Aliphatic C–H stretching
1,633	1,619	1°amine N–H bending

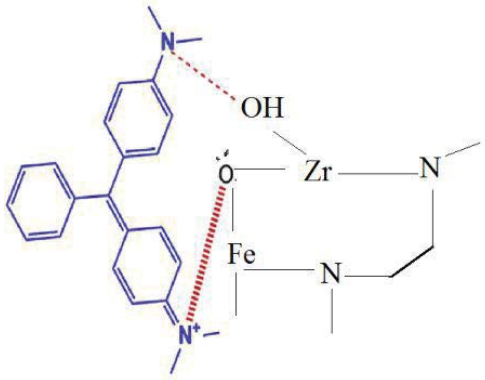

Fig. 5. Mechanism for the adsorption of MB on the composite material.

mixed oxide nanoparticle with ethylene diamine to form a composite material. Energy-dispersive X-ray spectroscopy (EDX) analysis showed the presence of constituent elements in free and dye loaded adsorbent. The binding of the dye molecules with the adsorbent surface was confirmed by the appearance of additional peak of sulfur (a constituent element of MB) in the spectrum of dye loaded adsorbent. The respective peaks of the elements before and after adsorption at the composite surface are shown in Figs. 6a and b.

Surface morphology was shown by the SEM images. Surface of the adsorbent before adsorption was spacious and less crowded while the surface becomes dense and packed with dye molecules after adsorption which is shown in Figs. 6c and d. The elemental composition of the material before and after adsorption is listed in Table 7.

3.9.4. BET Surface Area measurement

BET surface area suggests the area available for adsorption for the adsorbate molecules on the adsorbent surface. The surface area was estimated by BET method (N_2 adsorption in gaseous phase) using 0.0577 g of pre-dried sample at bath temperature of –195.96°C for 3 h at equilibration interval of 5 s. Surface area of the sample was found to be 54.74 $m^2\ g^{-1}$ before adsorption and 41.30 $m^2\ g^{-1}$ after adsorption. The decrease in surface area confirms dye adsorption.

3.9.5. Regeneration and reuse

Regeneration of any adsorbent is of utmost importance since it is linked with efficiency. Desorption was tested with

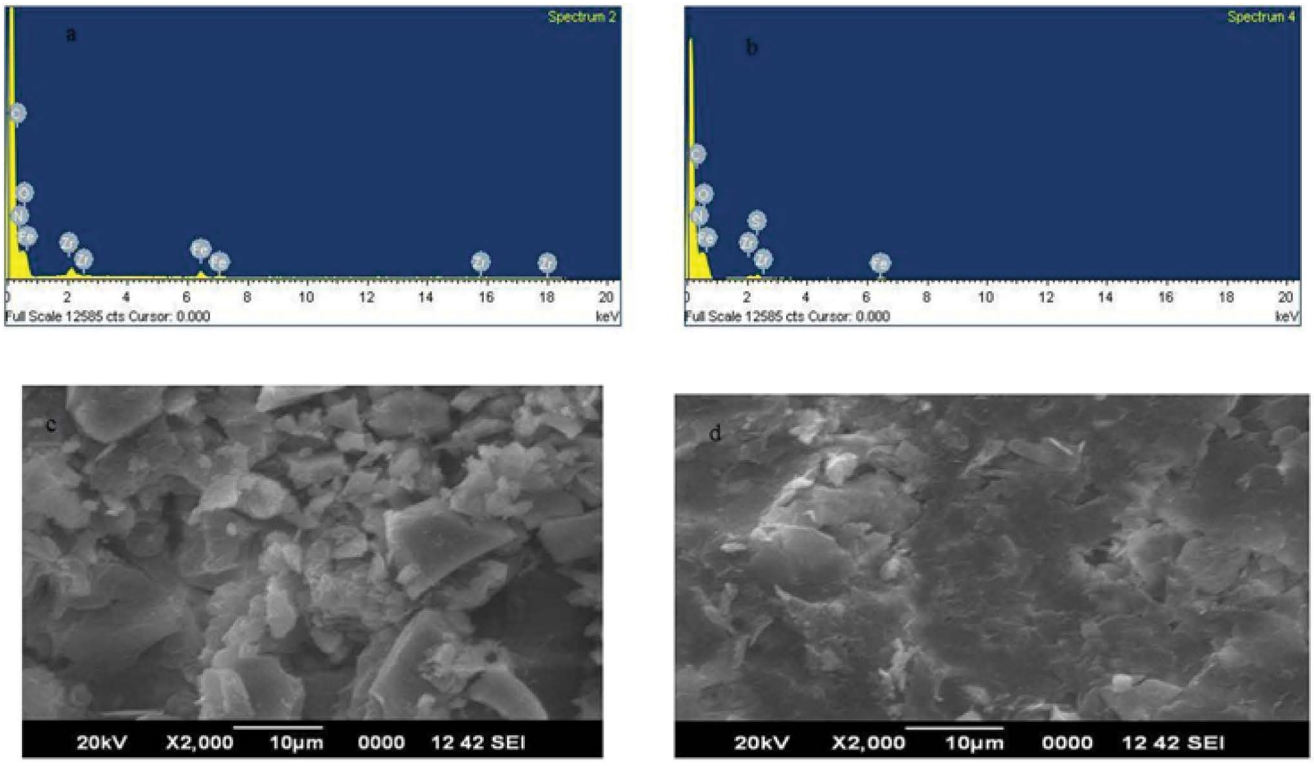

Fig. 6. (a) SEM of composite before adsorption, (b) SEM of composite after adsorption, (c) SEM morphology of composite before adsorption, and (d) SEM morphology of composite after adsorption.

Table 7
Comparison of elemental composition of the synthesized composite before and after adsorption

Before adsorption		After adsorption	
Element	Weight %	Element	Weight %
Carbon	14.91	Carbon	15.94
Oxygen	40.06	Oxygen	42.69
Iron	3.84	Iron	0.66
Zirconium	2.72	Zirconium	1.02
Nitrogen	38.47	Nitrogen	38.81
		Sulfur	0.86

Table 8
Real wastewater analysis in fixed-bed column mode using composite material

Parameters	Value
Adsorbent dose (g)	1
Effluent concentration (mg L^{-1})	1
Effluent (input) pH	8.2
Bed height (cm)	1.6
Radius (cm)	0.85
Flow rate (ml min^{-1})	8
Treated volume (ml)	800
Eluent (output) pH	7.4
Number of BV (bed volume)	220

*(1BV = 3.63 ml)

the dye loaded material in two different media (0.1 M HCl and 0.1 M NaOH). The desorption percent was calculated using the equation:

$$D\% = \frac{C_f}{C_i} \times 100 \quad (7)$$

where C_f and C_i are desorbed and adsorbed concentration respectively. Best desorption was obtained with 0.1 M HCl (79%) while for basic medium it was limited to 6%–8%. The higher desorption percent promotes the reusability of the material for the removal of cationic dye from wastewater.

3.9.6. Column study

Batch scale performance is required to be correlated with column performance to ascertain its suitability for field application. A fixed-bed column study was done using a glass column of diameter 17 cm. 1 L of artificial wastewater (2 mg L^{-1}) was passed through a fixed-bed height of 1.6 cm (1 g) at the flow rate of 8 ml min^{-1}. The treated effluent was collected at regular intervals and concentration was observed. The total volume rendered colourless was 600 mL which corresponds to 165 BV (1 BV = $\pi r^2 h$ = 3.63 mL). Column was then dismantled and the loaded adsorbent was tested for regeneration and re-use. Efficiency was found to get reduced only by 8%–10% in consecutive cycle.

3.9.7. Applications: real wastewater sample analysis

To evaluate the effectiveness of the material on commercial scale, a fixed-bed column experiment was conducted with real effluent collected from a local textile industry. The raw effluent was collected directly and was subjected to pretreatment which included sedimentation, filtration, centrifugation and neutralization. The treated effluent was highly alkaline as well as highly concentrated (high dye contamination). Hence, it was diluted several times and concentration was estimated before passing into the glass column for dye removal by IZBO-en. The parameters of the fixed-bed column mode along with the experimental data are listed in Table 8.

The volume detoxified using 1 g of composite material was 800 ml which corresponds to a bed volume of 220 BV that justified the practical novelty of the material on industrial scale.

4. Conclusion

The synthesis of IZBO-en composite material was simple and obtained with high yield (88%). FTIR, SEM and BET analysis showed the presence of active functional groups, porous nature of material and large surface area available for adsorption of MB. EDX showed the presence of dye in adsorbent. Batch study was conducted at different parameters like contact time, dose, pH, and dye concentration. Pseudo-second-order kinetic was followed with correlation coefficient of 0.998. The isotherm study suggested the process followed Langmuir model with maximum adsorption capacity of 242.79 mg g^{-1}. The thermodynamic study suggested the process to be feasible and spontaneous. The material was efficient for MB removal. Regeneration up to 79% was achieved in acidic medium which enhances the reusability of the material. Column study showed a remarkable efficiency (600 ml g^{-1}). Industrial wastewater sample analysis showed that 800 ml raw water can be decolourized by 1 g of adsorbent. It can be concluded that IZBO-en can be used in detoxification of dye contaminated water.

Acknowledgement

Authors thank Central University of Jharkhand for financial assistance and research facilities.

References

[1] J. Liu, H. Yang, S.N. Gosling, M. Kummu, M. Flörke, S. Pfister, N. Hanasaki, Y. Wada, X. Zhang, C. Zheng, T. Alcamo, T. Oki, Water scarcity assessments in the past, present and future, Earth's Future, 5 (2017) 545–559.
[2] Y.-Y. Jia, G.-J. Ren, A.-L. Li, L.-Z. Zhang, R. Feng, Y.-H. Zhang, X.-H. Bu, Temperature-Related synthesis of two anionic metal–organic frameworks with distinct performance in organic dye adsorption, Cryst. Growth Des., 16 (2016) 5593–5597.
[3] T. Matsuto, C.H. Jung, N. Tanaka, Material and heavy metal balance in a recycling facility for home electrical appliances, Waste Manage., 24 (2004) 425–436.
[4] B.H. Hameed, A.T.M. Din, A.L. Ahmad, Adsorption of methylene blue onto bamboo-based activated carbon: kinetics and equilibrium studies, J. Hazard. Mater., 141 (2007) 819–825.
[5] E. Forgacs, T. Cserháti, G. Oros, Removal of synthetic dyes from wastewaters: a review, Environ. Int., 30 (2004) 953–971.

[6] G.R. Bernardo, R.M. Rene, A.D. Ma Catalina, Chromium (III) uptake by agro-waste biosorbents: chemical characterization, sorption-desorption studies, and mechanism, J. Hazard. Mater., 170 (2009) 845–854.
[7] K.Vaaramaa, J. Lehto, Removal of metals and anions from drinking water by ion exchange, Desalination, 155 (2003) 157–170.
[8] X. Hu, Y. Li, Y. Wang, X. Li, H. Li, X. Liu, P. Zhang, Adsorption kinetics, thermodynamics and isotherm of thiacalix[4]arene-loaded resin to heavy metal ions, Desalination, 259 (2010) 76–83.
[9] B.A.M. Al-Rashdi, D.J. Johnson, N. Hilal, Removal of heavy metal ions by nanofiltration, Desalination, 315 (2013) 2–17.
[10] M. Petersková, C. Valderrama, O. Gibert, J.L. Cortina, Extraction of valuable metal ions (Cs, Rb, Li, U) from reverse osmosis concentrate using selective sorbents, Desalination, 286 (2012) 316–323.
[11] H. Javadian, Application of kinetic, isotherm and thermodynamic models for the adsorption of Co(II) ions on polyaniline/polypyrrole copolymer nanofibers from aqueous solution, J. Ind. Eng. Chem., 20 (2014) 4233–4241.
[12] M. Soleimani Lashkenari, B. Davodi, M. Ghorbani, H. Eisazadeh, Use of core-shell polyaniline/polystyrene nanocomposite for removal of Cr (VI), High Perform. Polym., 24 (2012) 345–355.
[13] S. Jitjaicham, P. Kampalanonwat, P. Supaphol, Metal adsorption behavior of 2,4-dinitrophenyl hydrazine modified polyacrylonitrile nanofibers, eXPRESS Polym. Lett., 7 (2013) 832–841.
[14] L. Li, Y. Li, X. Luo, J. Deng, W. Yang, Helical poly (*N*-propargylamide)s with functional catechol groups: synthesis and adsorption of metal ions in aqueous solution, React. Funct. Polym., 70 (2010) 938–943.
[15] J. Huang, K. Zhang, The high flux poly (m-phenylene isophthalamide) nanofiltration membrane for dye purification and desalination, Desalination, 282 (2011) 19–26.
[16] N. Yang, S. Zhu, D. Zhang, S. Xu, Synthesis and properties of magnetic Fe_3O_4-activated carbon nanocomposite particles for dye removal, Mater. Lett., 62 (2008) 645–647.
[17] L. Ai, H. Huang, Z. Chen, X. Wei, J. Jiang, Activated carbon/$CoFe_2O_4$ composites: facile synthesis, magnetic performance and their potential application for the removal of malachite green from water, Chem. Eng. J., 156 (2010) 243–249.
[18] G. Zhang, J. Qu, H. Liu, A.T. Cooper, R. Wu, $CuFe_2O_4$/activated carbon composite: a novel magnetic adsorbent for the removal of acid orange II and catalytic regeneration, Chemosphere, 68 (2007) 1058–1066.
[19] I.D. Mall, V.C. Srivastava, N.K. Agarwal, Removal of Orange-G and Methyl Violet Dyes by adsorption onto bagasse fly ash—Kinetic study and equilibrium isotherm analyses, Dyes Pigm., 69 (2006) 210–233.
[20] X. Ren, W. Xiao, R. Zhang, Y. Shang, R. Han, Adsorption of crystal violet from aqueous solution by chemically modified phoenix tree leaves in batch mode, Desal. Water Treat., 53 (2015) 1324–1334.
[21] R. Sankar, M. Sasidaran, T. Kaliyappan, Synthesis, characterization, thermal and chelation properties of new polymeric hydrazone based on 2,4-dihydroxy benzaldehyde, High Perform. Polym., 23 (2011) 32–39.
[22] M.V. Dinu, E.S. Dragan, Heavy metals adsorption on some iminodiacetate chelating resins as a function of the adsorption parameters, React. Funct. Polym., 68 (2008) 1346–1354.
[23] M. Sasidaran, R. Sankar, P. Kandasamy, S. Vijayalakshmi, T. Kaliyappan, Chelating and biological properties of an azo polymer resin: synthesis, characterization and its application, High Perform. Polym., 23 (2011) 602–609.
[24] I.F. Mironyuk, V.M. Gun'ko, H.V. Vasylyeva, O.V. Goncharuk, T.R. Tatarchuk, V.I. Mandzyuk, N.A. Bezruka, T.V. Dmytrotsa, Effects of enhanced clusterization of water at a surface of partially silylated nanosilica on adsorption of cations and anions from aqueous media, Microporous Mesoporous Mater., 277 (2019) 95–104.
[25] A.A. El-Fadl, A.M. Hassan, M.H. Mahmoud, T. Tatarchuk, I.P. Yaremiy, A.M. Gismelssed, M.A. Ahmed, Synthesis and magnetic properties of spinel $Zn_{1-x}Ni_xFe_2O_4$ (0.0≤x≤1.0) nanoparticles synthesized by microwave combustion method, J. Magn. Magn. Mater., 471 (2019) 192–199.
[26] M.A. Ahmed, H.E. Hassan, M.M. Eltabey, K. Latka, T.R. Tatarchuk, Mossbauer spectroscopy of $Mg_xCu_{0.5-x}Zn_{0.5}Fe_2O_4$ (x = 0.0, 0.2 and 0.5) ferrites system irradiated by γ-rays, Phys. B Condens. Matter., 530 (2018) 195–200.
[27] Mu. Naushad, Z.A. Alothman, M.R. Awual, S.M. Alfadul, T. Ahamad, Adsorption of rose Bengal dye from aqueous solution by amberlite Ira-938 resin: kinetics, isotherms, and thermodynamic studies, Desal. Water Treat., 57 (2016) 13527–13533.
[28] L. Gnanasekaran, R. Hemamalini, Mu. Naushad, Efficient photocatalytic degradation of toxic dyes using nanostructured TiO_2/polyaniline nanocomposite, Desal. Water Treat., 108 (2018) 322–328.
[29] A.B. Albadarin, M.N. Collins, Mu. Naushad, S. Shirazian, G. Walker, C. Mangwandi, Activated lignin-chitosan extruded blends for efficient adsorption of methylene blue, Chem. Eng. J., 307 (2017) 264–272.
[30] T. Tatarchuk, M. Bououdina, B. Al-Najar, R.B. Bitra, Green and Ecofriendly Materials for the Remediation of Inorganic and Organic Pollutants in Water, M. Naushad Eds., A New Generation Material Graphene: Applications in Water Technology, Springer, Cham, 2019, pp. 69–110.
[31] A.A. Alqadami, Mu. Naushad, M.A. Abdalla, M.R. Khan, Z.A. Alothman, Adsorptive removal of toxic dye using Fe_3O_4–TSC nanocomposite: equilibrium, kinetic, and thermodynamic studies, J. Chem. Eng. Data, 61 (2016) 3806–3813.
[32] A.A. Alqadami, Mu. Naushad, Z.A. Alothman, T. Ahamad, Adsorptive performance of MOF nanocomposite for methylene blue and malachite green dyes: kinetics, isotherm and mechanism, J. Environ. Manage., 223 (2018) 29–36.
[33] J. Han, J. Dai, R. Guo, Highly efficient adsorbents of poly (*o*-phenylenediamine) solid and hollow sub-microspheres towards lead ions: a comparative study, J. Colloid Interface Sci., 356 (2011) 749–756.
[34] H. Javadian, M.T. Angaji, Mu. Naushad, Synthesis and characterization of polyaniline/g-alumina nanocomposite: a comparative study for the adsorption of three different anionic dyes, J. Ind. Eng. Chem., 25 (2014) 3890–3900.
[35] M.H. Beyki, M. Shirkhodaie, M.A. Karimi, M.J. Aghagoli, F. Shemirani, Green synthesized Fe_3O_4 nanoparticles as a magnetic core to prepare poly 1, 4 phenylenediamine nanocomposite: employment for fast adsorption of lead ions and azo dye, Desal. Water Treat., 57 (2016) 28875–28886.
[36] E. Daneshvar, A. Vazirzadeh, A. Niazi, M. Kousha, Mu. Naushad, A. Bhatnagar, Desorption of Methylene blue dye from brown macroalga: effects of operating parameters, isotherm study and kinetic modeling, J. Cleaner Prod., 152 (2017) 443–453.
[37] T.N.V. D. de Souza, S.M.L. de Carvalho, M.G.A. Vieira, M.G.C. da Silva, D. do Socorro Barros Brasil, Adsorption of basic dyes onto activated carbon: experimental and theoretical investigation of chemical reactivity of basic dyes using DFT-based descriptors, Appl. Surf. Sci., 448 (2018) 662–670.
[38] R. Ianoş, C. Păcurariu, S.G. Muntean, E. Muntean, M.A. Nistor, D. Nižňanský, Combustion synthesis of iron oxide/carbon nanocomposites, efficient adsorbents for anionic and cationic dyes removal from wastewaters, J. Alloys Compd., 741 (2018) 1235–1246.
[39] C. Păcurariu, O. Paşka, R. Ianoş, S.G. Muntean, Effective removal of methylene blue from aqueous solution using a new magnetic iron oxide nanosorbent prepared by combustion synthesis, Clean Technol. Environ. Policy, 18 (2016) 705–715.
[40] S.G. Muntean, A. Todea, M.E. Rădulescu-Grad, A. Popa, Decontamination of colored wastewater using synthetic sorbents, Pure Appl. Chem., 86 (2014) 1771–1780.
[41] S.G. Muntean, A. Todea, S. Bakardjieva, C. Bologa, Removal of non benzidine direct red dye from aqueous solution by using natural sorbents: *Beech* and *Silver Fir*, Desal. Water Treat., 66 (2017) 235–250.
[42] S. Ming-Twang, M.A.A. Zaini, L. Md. Salleh, Mohd. A.C. Yunus, Mu. Naushad, Potassium hydroxide-treated palm kernel shell

sorbents for the efficient removal of methyl violet dye, Desal. Water Treat., 84 (2017) 262–270.
[43] N.M. Mahmoodi, Z. Hosseinabadi-Farahani, H. Chamani, Dyes adsorption from single and binary systems using NiO-MnO_2 nanocomposite and artificial neutral network modelling, Environ. Prog. Sustainable Energy, 36 (2016) 111–119.
[44] Y.-S. Ho, Isotherms for the sorption of lead onto peat: comparison of linear and non-linear methods, Pol. J. Environ. Stud., 15 (2006) 81–86.
[45] C. Li, Z. Xiong, J. Zhang, C. Wu, The strengthening role of the amino group in metal–organic framework MIL-53 (Al) for methylene blue and malachite green dye adsorption, J. Chem. Eng. Data, 60 (2015) 3414–3422.
[46] Y. Shao, L. Zhou, C. Bao, J. Ma, M. Liu, F. Wang, Magnetic responsive metal–organic frameworks nanosphere with core–shell structure for highly efficient removal of methylene blue, Chem. Eng. J., 283 (2016) 1127–1136.
[47] E. Haque, V. Lo, A.I. Minett, A.T. Harris, T.L. Church, Dichotomous adsorption behaviour of dyes on an amino-functionalised metal–organic framework, amino-MIL-101(Al), J. Mater. Chem. A, 2 (2014) 193–203.
[48] F. Ge, H. Ye, M.-M. Li, B.-X. Zhao, Efficient removal of cationic dyes from aqueous solution by polymer-modified magnetic nanoparticles, Chem. Eng. J., 198 (2012) 11–17.
[49] O.A. Attallah, M.A. Al-Ghobashy, M. Nebsen, M.Y. Salem, Removal of cationic and anionic dyes from aqueous solution with magnetite/pectin and magnetite/silica/pectin hybrid nanocomposites: kinetic, isotherm and mechanism analysis, RSC Adv., 6 (2016) 11461–11480.
[50] E.I. El-Shafey, S.N.F. Ali, S. Al-Busafi, H.A.J. Al-Lawati, Preparation and characterization of surface functionalized activated carbons from date palm leaflets and application for methylene blue removal, J. Environ. Chem. Eng., 4 (2016) 2713–2724.
[51] O.M. Paşka, C. Păcurariu, S.G. Muntean, Kinetic and thermodynamic studies on methylene blue biosorption using corn-husk, RSC Adv., 107 (2014) 62621–62630.
[52] S.N. Kane, S. Raghuvanshi, M. Satalkar, V.R. Reddy, U.P. Deshpande, T.R. Tatarchuk, F. Mazaleyrat, Synthesis, Characterization and Antistructure Modeling of Ni Nano Ferrite, AIP Conference Proceedings, 1953 (2018) ID: 030089.
[53] B.R. Babu, T. Tatarchuk, Elastic properties and antistructural modeling for Nickel-Zinc ferrite-aluminates, Mater. Chem. Phys., 207 (2018) 534–541.
[54] A.A. Alqadami, Mu. Naushad, Z.A. Alothman, A.A. Ghfar, Novel metal–organic framework (MOF) based composite material for the sequestration of U(VI) and Th(IV) metal ions from aqueous environment, ACS Appl. Mater. Interfaces, 9 (2017) 36026–36037.